ACS APPLIED MATERIALS & INTERFACES

Research Article

www.acsami.org

Role of Cu in Mo_6S_8 and Cu Mixture Cathodes for Magnesium Ion Batteries

Seung-Hyun Choi,[†,∥] Jeom-Soo Kim,[‡] Sang-Gil Woo,[†] Woosuk Cho,[†] Sun Yong Choi,[§] Jungkyu Choi,[∥,⊥] Kyu-Tae Lee,*[,#] Min-Sik Park,*[,†] and Young-Jun Kim[†]

[†]Advanced Batteries Research Center, Korea Electronics Technology Institute, Seongnam, Gyeonggi 463-816, Republic of Korea

[‡]Department of Chemical Engineering, Dong-A University, Busan 604-714, Republic of Korea

[§]Cheorwon Plasma Research Institute, Cheorwon, Gangwon 269-802, Republic of Korea

[∥]Department of Chemical and Biological Engineering, Korea University, Seoul 136-701, Republic of Korea

[⊥]Green School, Korea University, Seoul 136-701, Republic of Korea

[#]School of Chemical and Biological Engineering, Seoul National University, Seoul 151-744, Republic of Korea

Supporting Information

ABSTRACT: The reversible capacity of Chevrel Mo_6S_8 cathode can be increased by the simple addition of the Cu metal to Mo_6S_8 electrodes. However, the exact reaction mechanism of the additional reversible capacity for the Mo_6S_8 and Cu mixture cathode has not been clearly understood yet. To clarify this unusual behavior, we synthesize a novel Cu nanoparticle/graphene composite for the preparation of the mixture electrode. We thoroughly investigate the electrochemical behaviors of the Mo_6S_8 and Cu mixture cathode with the relevant structural verifications during Mg^{2+} insertion and extraction. The *in situ* formation of $Cu_xMo_6S_8$ is observed, indicating the spontaneous electrochemical insertion of Cu to the Mo_6S_8 host from the Cu nanoparticle/graphene composite. The reversible electrochemical replacement reaction of Cu in the Mo_6S_8 structure is clarified with the direct evidence for the solid state Cu deposition/dissolution at the surface of Mo_6S_8 particles. Moreover, the Mo_6S_8 and Cu mixture cathode improves the rate capability compared to the pristine. We believe that our finding will contribute to understanding the origin of the additional capacity of the Mo_6S_8 cathode arising from Cu addition and improve the electrochemical performance of the Mo_6S_8 cathode for rechargeable Mg batteries.

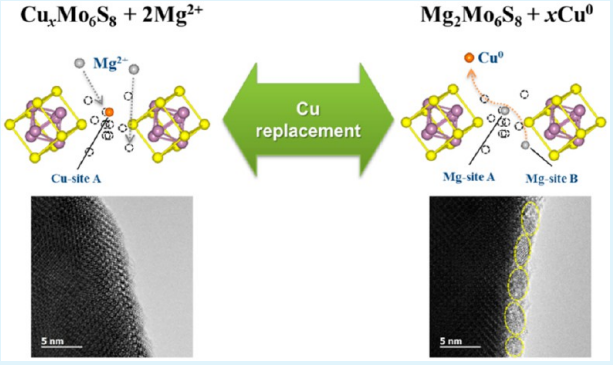

KEYWORDS: *Chevrel Mo_6S_8, Cu nanoparticle/graphene composite, cathode, Mg batteries, electrochemistry*

INTRODUCTION

In order to solve the current energy issues, there is a crucial need for energy storage technology capable of maximizing the efficiency of integrating renewable energy sources, resolving the intermittency problems associated with renewable sources, and minimizing energy loss by more closely matching supply and demand.[1−5] Although lithium-ion batteries (LIBs) have proven to be the most popular option for the efficient storage of electrical energy in the form of chemical energy, they currently suffer from high production costs and poor operational safety.[6−8] Expanding their application to large-scale energy storage systems is therefore dependent on further improvements in these areas.

Given the current limitations of LIBs, rechargeable magnesium (Mg) batteries have been identified as a possible future energy storage technology because of their high theoretical capacity, good operational safety, and the relative abundance of Mg.[9−11] However, there are still many technical challenges that need to be resolved before they can be successfully implemented. In recent years, there has been considerable research into discovering new cathode materials that can reversibly host Mg^{2+} within their structure, as well as electrolytes with a suitable functionality of Mg metal deposition/dissolution across a wide voltage window.[12,13]

The Chevrel-phase Mo_6S_8 has received particular attention as a promising cathode material for commercial use in rechargeable Mg batteries due to their excellent cycle performance and power characteristics. Its reversible capacity, however, has so far been limited to less than 100 mAh/g, with a low reaction potential of around 1.0 V vs Mg/Mg^{2+}. There is therefore clearly a need to further improve the reversible capacity of Mo_6S_8,[14−16] and many researchers have focused on

Received: February 9, 2015
Accepted: March 10, 2015
Published: March 10, 2015

DOI: 10.1021/am508702j
ACS Appl. Mater. Interfaces 2015, 7, 7016−7024

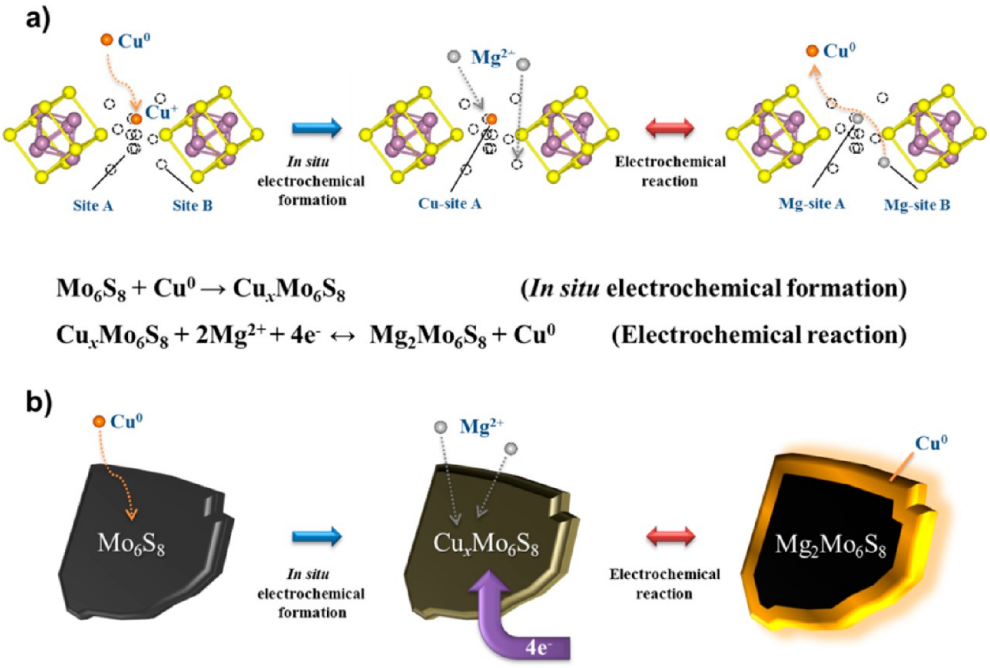

Figure 1. Schematics of (a) Cu replacement reaction in the Mo_6S_8 and (b) the proposed solid state Cu replacement reaction structure during Mg^{2+} insertion and extraction.

morphological or structural modification as a means to achieve this.[17−19] Remarkable progress in this regard was achieved by Aurbach and co-workers when they discovered the positive effect of residual Cu in the $Cu_xMo_6S_8$ structure on its electrochemical performance. They subsequently suggested that Cu can be extracted from the $Cu_xMo_6S_8$ structure by Mg^{2+} insertion and that the reversible involvement of this extracted Cu in the electrochemical reaction with Mo_6S_8 leads to an increment in the reversible capacity.[20,21] Recently, it also has been found that the simple addition of elemental Cu into a Mo_6S_8 cathode creates a very similar electrochemical behavior to the $Cu_xMo_6S_8$ cathode.[22] Inspired by this unexpected finding, consideration was given to whether the additional capacity achieved with the addition of Cu reflects a spontaneous response associated with elemental Cu incorporated in the cathode during cycling. Despite these interesting observations, there has yet been no further investigation into this matter.

Clearly, identifying the incomplete reaction mechanism of Cu replacement is regarded as the most urgent issue for further improvement of the Mo_6S_8 cathode. On the basis of previous inferences, we develop a Cu nanoparticle/graphene composite as a functional additive for systematic investigation. In order to maximize the electrochemical activity, Cu nanoparticles were successfully anchored on the surface of a graphene framework by high-temperature plasma synthesis. This proposed concept is intended to secure a sufficient active Cu surface area by suppressing undesirable agglomeration, while also ensuring electrical conduction through the graphene framework. First of all, we herein present an assessment of its feasibility for increasing the reversible capacity of a conventional Mo_6S_8 cathode. We also investigate structural changes of the Mo_6S_8 in the cathode containing the Cu nanoparticle/graphene composite additive during Mg^{2+} insertion and extraction. From various structural and electrochemical observations, we suggest a possible reaction mechanism of Cu replacement in the Mo_6S_8 structure with a structural viewpoint. Furthermore, our hypothesis has been clearly proved with direct evidence.

EXPERIMENTAL SECTION

Material Synthesis. Chevrel-phase $Cu_{2.5}Mo_6S_8$ was synthesized by a controlled solid state reaction with a stoichiometric mixture of Cu (1.288 g, Aldrich, 99.7%), MoS_2 (5.224 g, Aldrich, 99.0%), and Mo (1.552 g, Aldrich, 99.9%) precursor powders prepared by mechanical milling at 480 rpm for 6 h under an Ar atmosphere. A custom-made sealed reactor was filled with this as-prepared powder and then heated at 1100 °C for 24 h under an Ar atmosphere. In order to remove Cu from the structure of the resulting powder, it was chemically etched in 6 M hydrochloric acid (HCl) solution with O_2 bubbling for 6 h and then washed with deionized water. After drying at 80 °C for 12 h in a vacuum oven, the final product was collected and ground before use. A Cu nanoparticle/graphene composite was also produced by high-temperature plasma synthesis, in which a mixture of Cu powder (∼30 μm, 2 g) and graphene (∼5 μm, 10 g) after mechanical milling at 480 rpm for 2 h was fed into a plasma reactor with a N_2 carrier gas. A schematic diagram depicting this process is given in Figure S2, Supporting Information.

Structural Characterizations. The morphology and microstructure of the Mo_6S_8 cathode material and Cu nanoparticle/graphene composite additive were examined using field-emission scanning electron microscopy (FESEM, JEOL JSM-7000F) and high-resolution transmission electron microscopy (HRTEM, JEOL ARM-200F) combined with energy dispersive X-ray spectroscopy (EDS). Powder X-ray diffraction (XRD) patterns were obtained using an X-ray diffractometer (PANanalytical, Empyrean) equipped with a 3D pixel semiconductor detector and a Cu Kα radiation source (λ = 1.54056 Å). Further structural characterizations were performed using a Raman spectrometer (Bruker Senterra Grating 400) with a He−Ne laser at a wavelength of 532 nm and by X-ray photoelectron spectroscopy (XPS, Thermo Scientific Sigma Probe). The composition of the Cu nanoparticle/graphene composite was confirmed by thermogravimetric analysis (TGA, PerkinElmer TG/DTA 6300).

Electrochemical Measurements. The cathodes were prepared by coating stainless steel foils with a slurry containing Mo_6S_8 powder (70 wt %), conducting agent (Super-P, 20 wt %), and polyvinylidene fluoride binder (PVdF, 10 wt %) dissolved in *N*-methyl-2-pyrrolidone

DOI: 10.1021/am508702j
ACS Appl. Mater. Interfaces 2015, 7, 7016−7024

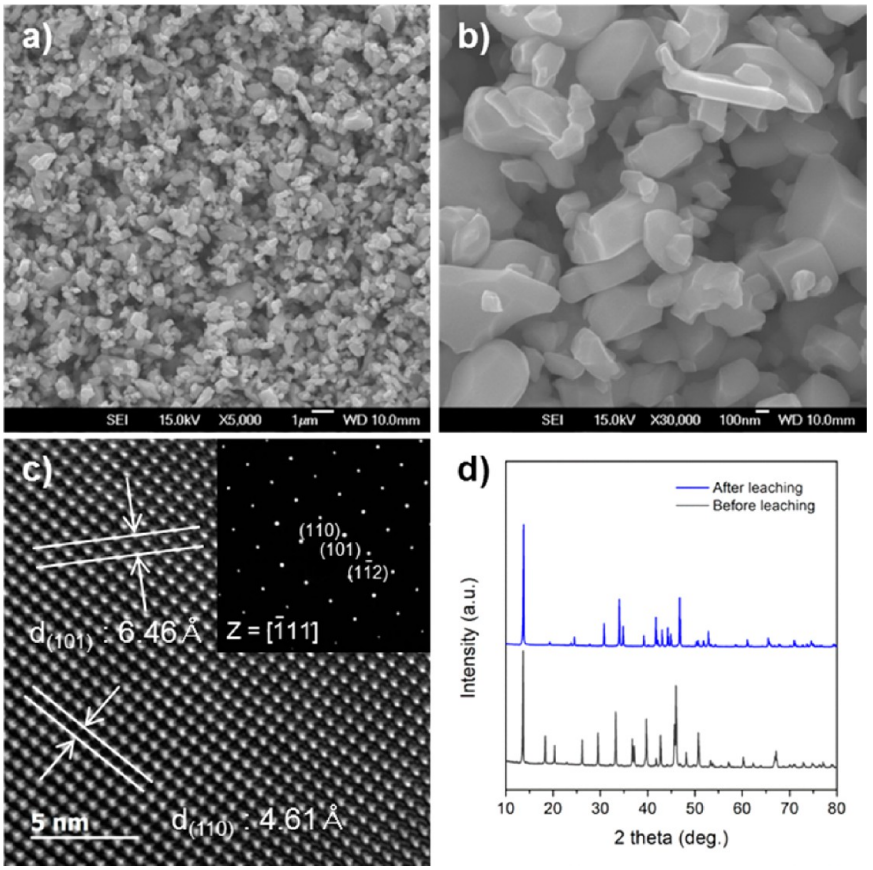

Figure 2. (a, b) FESEM images of Mo_6S_8 at different magnifications. (c) High-resolution TEM image of Mo_6S_8 and its corresponding selected area diffraction pattern. (d) Powder XRD patterns of $Cu_{2.5}Mo_6S_8$ and Mo_6S_8 after chemical leaching with a 6 M HCl solution.

(NMP). For comparative purposes, cathodes with Mo_6S_8 powder (65.6 wt %), Cu nanoparticle/graphene composite, or Si nanoparticle/graphene composite (16.4 wt %), Super-P (10 wt %), and PVdF binder (8 wt %) dissolved in NMP solution were also prepared in the same manner. After coating, the cathodes were dried at 120 °C for 10 h and were then pressed under a pressure of 200 kg/cm^2. The loading amount and density of the cathodes were fixed at 1.6 mg/cm^2 and 2.7 g/cm^3, respectively. Next, 2032 coin cells were carefully assembled in an Ar-filled glovebox using two porous cellulose membranes as separators and an electrolyte of 0.4 M $(PhMgCl)_2$-$AlCl_3$ in tetrahydrofuran (THF) solvent. A Mg metal disk (diameter: 15 mm; thickness: 1 mm) was used as an anode, and native MgO film on the disk was carefully removed by polishing in a Ar-filled glovebox before use. These cells were then galvanostatically discharged (Mg^{2+} insertion) and charged (Mg^{2+} extraction) within a voltage range of 0.5 to 1.95 V vs Mg/Mg^{2+} at different current densities in order to evaluate their electrochemical performance at room temperature.

RESULTS AND DISCUSSION

Not only Mo_6S_8 but also $Cu_xMo_6S_8$ is capable of hosting divalent Mg^{2+} in the structure, where Cu is occupied in A sites of the Mo_6S_8 structure.[20,21] Figure 1a describes a schematic of electrochemical replacement reaction of Cu in the Chevrel Mo_6S_8 structure during Mg^{2+} insertion and extraction.[21] Recently, our group observed the *in situ* formation of $Cu_xMo_6S_8$, when Cu metal particles are externally provided for the preparation of the electrode using a pure phase Mo_6S_8.[22] From those findings, it is definite that Cu can be electrochemically reacted with Mo_6S_8. Furthermore, Cu is diffused out from the $Cu_xMo_6S_8$ in parallel with Mg^{2+} insertion, and the extracted Cu is reversibly reinserted by subsequent Mg^{2+} extraction during cycles. Inspired by these works, we examined the reaction mechanism of the electrode comprised of Mo_6S_8 and Cu metal, particularly focusing on Cu destination at the final stage of the reaction. We first propose a possible reaction mechanism of Cu replacement in the Mo_6S_8 structure, as described in Figure 1b. When Cu metal and Mo_6S_8 are electrically shorted in the electrolyte, Mo_6S_8 is self-discharged with the spontaneous intercalation of Cu in the Mo_6S_8 structure. Then, during the discharge (insertion of Mg^{2+}), the Cu^+ is diffused out by electrochemical replacement with Mg^{2+} and reduced to Cu^0 through the deposition on the surface of the Mo_6S_8 particles. During charge (extraction of Mg^{2+}), Cu^0 is oxidized and reversibly inserted to the host structure occupying available sites as a result of Mg^{2+} extraction. For the experimental verification of our proposal, we prepared the pure phase Mo_6S_8 and Cu nanoparticle/graphene composite as an external Cu source. The Cu nanoparticle/graphene composite, in which Cu nanoparticles are uniformly anchored on the graphene framework, was designed with a purpose of providing Cu in the cathode. Its distinctive morphology would be advantageous for maximizing reactivity of Cu by suppressing undesirable agglomeration and securing sufficient electrical conduction.

Figure 2a,b shows FESEM images of Mo_6S_8 powder at different magnifications, clearly indicating that the particles range in size from 100 to 500 nm and are effectively isolated from each other. A high-resolution TEM observation (Figure 2c) with the accompanying selected area electron diffraction (SAED) pattern reveals that the Mo_6S_8 has a fine rhombohedral microstructure with a space group of $R\bar{3}$.[23] Mg^{2+} ions are

DOI: 10.1021/am508702j
ACS Appl. Mater. Interfaces 2015, 7, 7016−7024

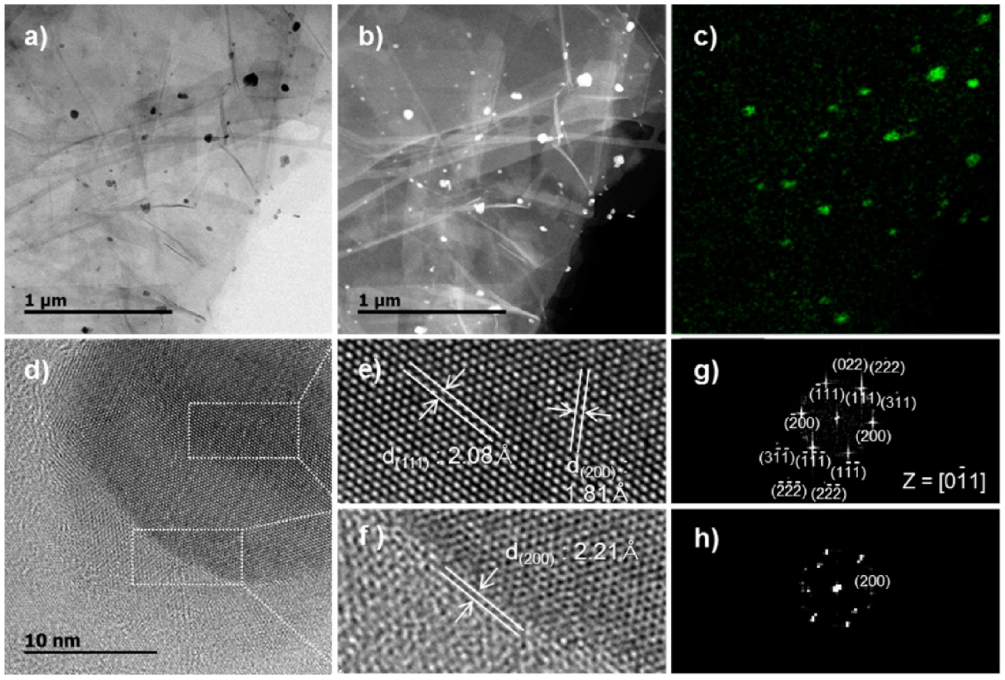

Figure 3. (a) Bright-field and (b) dark-field TEM images of Cu nanoparticle/graphene composite. (c) Corresponding EDS elemental mapping of Cu. (d) High-resolution TEM image of a Cu nanoparticle in Cu nanoparticle/graphene composite and magnified TEM images of a Cu nanoparticle in the (e) bulk region and (f) surface region with (g, h) calculated FFT patterns.

accommodated within the Mo_6 framework of a Chevrel-phase Mo_6S_8 structure.[24] Moreover, according to the powder XRD pattern in Figure 2d, the pure phase Mo_6S_8 having a rhombohedral structure was obtained without impurities (JCPDS 27-0319). The lattice parameters were calculated to be $a = b = 9.186(5)$ and $c = 10.89(1)$, both of which are in good agreement with the previous work.[25] For comparison, the morphology and microstructure of the $Cu_{2.5}Mo_6S_8$ prior to chemical etching are given in Figure S1, Supporting Information.

A Cu nanoparticle/graphene composite was synthesized by a high-temperature plasma process at optimized conditions, and FESEM images indicate that abundant Cu nanoparticles are uniformly deposited over the surface of a graphene framework (Figure S2, Supporting Information). Furthermore, the bright-field (Figure 3a) and dark-field TEM (Figure 3b) images, as well as the EDS elemental mapping result in Figure 3c, confirm that these Cu nanoparticles are less than 10 nm in size and are effectively anchored on the surface of the graphene framework. It is considered likely that this strong binding between the Cu nanoparticles and graphene framework is a direct result of the high-temperature of processing. High-resolution TEM observations identified the microstructure of individual Cu nanoparticles (Figure 3d), revealing a *d*-spacing of 2.08 Å in the bulk material (Figure 3e) and a trace of CuO with a *d*-spacing of 2.21 Å observed on the surface (Figure 3f). Both of these results are in good agreement with their respective fast Fourier transform (FFT) results (Figure 3g,h).[26]

The microstructure of the Cu nanoparticle/graphene composite was further investigated by XRD analysis, the result of which is shown in Figure S3a, Supporting Information. The distinct peaks of the composite at $2\theta = 43.3°$, 50.5°, and 74.2° correspond to the (111), (200), and (220) planes of crystalline Cu, respectively. Interestingly, there is also a notable growth of the graphene (002) peak at $2\theta = 26.6°$, which may be caused by a restacking of the graphene framework during high-temperature synthesis. Figure S3b, Supporting Information, shows the Raman spectra of the Cu nanoparticle/graphene composite, in which three Raman bands at 1348, 1579, and 2710 cm^{-1} are characteristic of the D-band, G-band, and 2D-band of graphene, respectively.[27,28] However, compared to the spectra of pristine graphene, there is a slight increase evident in the G-band. The intensity ratio (I_D/I_G) is therefore slightly decreased from 0.293 to 0.258, providing further evidence of graphene restacking under high temperature.[29] In the TGA analysis result (Figure S3c, Supporting Information), it should be noted that approximately 11.5 wt % of Cu or Cu oxides was found in the Cu nanoparticle/graphene composite. Figure S3d, Supporting Information, shows XPS spectra collected from the Cu nanoparticle/graphene composite after careful correction of the charging based on a C 1s excitation at 284.5 eV. With this, we found that the Cu 2p spectra exhibits two dominant signals at 952.6 eV ($2P_{1/2}$) and 932.9 eV ($2P_{3/2}$) with the deconvoluted results revealing that both peaks are mainly attributed to metallic Cu (Cu^0) and partial oxides (Cu^+ and Cu^{2+}).[30] Moreover, chemically/electrochemically inactive Si nanoparticle/graphene composite was prepared by the same method (Figures S4 and S5, Supporting Information) to provide a useful reference for determining the precise role of Cu in the composite.

The effect of Cu nanoparticle/graphene composite on the electrochemical performance of the Mo_6S_8 cathode was investigated using 2032 coin-type cells. The cells were initially discharged to 0.5 V vs Mg/Mg^{2+} for Mg^{2+} insertion (Figure 4a) and then subsequently charged and discharged in a voltage range of 0.5 to 1.95 V vs Mg/Mg^{2+}. Figure 4b shows subsequent charge (Mg^{2+} extraction) and discharge (Mg^{2+} insertion) profiles of Mo_6S_8 cathode containing Cu nanoparticle/graphene composite as an additive. This shows that, while the pristine cell exhibits a discharge capacity of only 85.6

DOI: 10.1021/am508702j
ACS Appl. Mater. Interfaces 2015, 7, 7016−7024

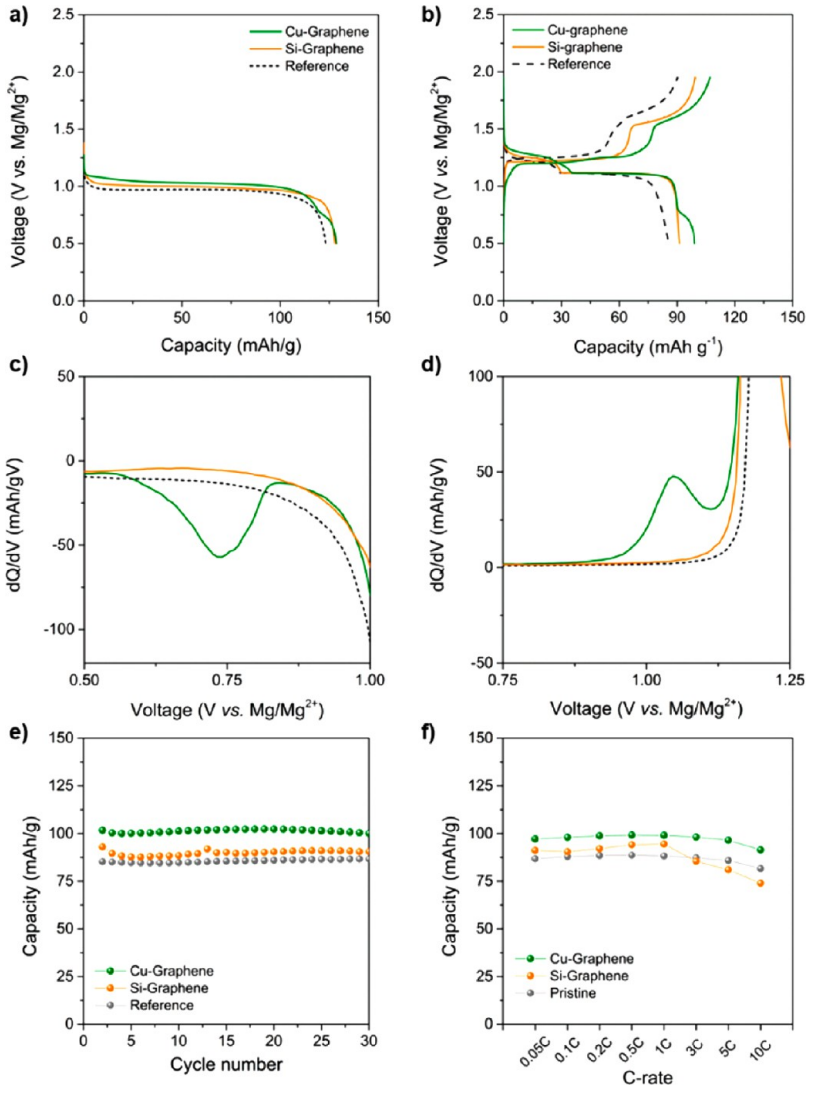

Figure 4. (a) Galvanostatic initial discharge profiles and (b) subsequent charge and discharge profiles of the Mo_6S_8 cathode containing a Cu nanoparticle/graphene composite within a voltage range of 0.5 to 1.95 V vs Mg/Mg^{2+} at a constant current of 0.05 C (6 mA/g). The dQ/dV profiles of the cell during (c) discharging to 0.5 V vs Mg/Mg^{2+} and (d) charging to 1.95 V vs Mg/Mg^{2+}. (e) Cycle performance of a cell containing a Cu nanoparticle/graphene composite within a voltage range of 0.5 to 2.0 V vs Mg/Mg^{2+} at a constant current of 0.05 C (6 mA/g) and (f) its rate capability at current densities ranging from 0.05 to 10 C (1 C = 120 mA/g).

mAh/g, with a single plateau at 1.0 V vs Mg/Mg^{2+}, a higher discharge capacity of 99.1 mAh/g is attained with the addition of Cu nanoparticle/graphene composite, creating a new plateau at 0.75 V vs Mg/Mg^{2+}. Note that this is a very similar electrochemical behavior to that observed with $Cu_xMo_6S_8$ obtained by incomplete chemical leaching.[21] For comparison, the effect of inactive Si nanoparticle/graphene composite additive was also investigated, which not surprisingly failed to find any discernible electrochemical contribution from Si. The slight increase observed in the discharge capacity (91.3 mAh/g) when using a Si nanoparticle/graphene composite is attributed to the improved electrical conduction of the graphene framework.

The additional capacity obtained during charging by adding Cu nanoparticle/graphene composite was also evident in the initial stage of the subsequent discharge, thus indicating that the electrochemical replacement reaction of Cu is fully reversible. The additional reactions allowed by the Cu nanoparticle/graphene composite are also obvious in the corresponding dQ/dV curves, in which a reduction peak is clearly observed at 0.75 V vs Mg/Mg^{2+} during discharge (Figure 4c) and a corresponding oxidation peak appears at 1.05 V vs Mg/Mg^{2+} during charging (Figure 4d). This redox reaction is definitely not caused by the corrosion of Cu metal, because the reduction peak was observed at the first cycle, indicating Cu^+ already exists prior to oxidation of the composite (Figure S6, Supporting Information). Note that no reduction peak was observed for the pristine and Si nanoparticle/graphene composite electrodes at the first cycle. In addition, there is no evidence for any other side reactions being involved in the given system, at least within the operating voltage window (Figure S7, Supporting Information).

Figure 4e shows the cycle performance of the cells at a constant current of 0.1 C (1 C = 120 mA/g), in which the additional capacity is maintained without significant capacity fading after 30 cycles indicating that the electrochemical replacement of Cu in the cell is fully reversible. Although Figure 4f seems to show a similar rate performance of the electrodes, it is notable that the addition of Cu nanoparticle/graphene composite reduces the polarization compared to the pristine,

DOI: 10.1021/am508702j
ACS Appl. Mater. Interfaces 2015, 7, 7016−7024

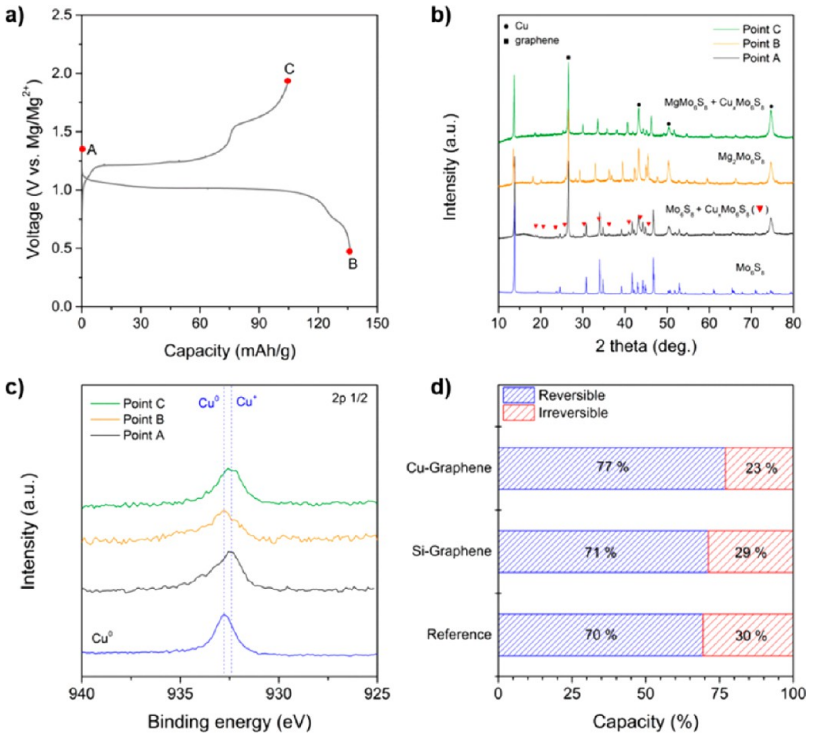

Figure 5. (a) Galvanostatic charge and discharge profiles of a cell containing a Cu nanoparticle/graphene composite in the first cycle; (i) OCV (point A), (ii) after Mg^{2+} insertion (point B), and (iii) after Mg^{2+} extraction (point C). (b) *Ex situ* XRD patterns (see Figure S9, Supporting Information) and (c) *ex situ* XPS Cu 2p spectra collected from the cathodes containing a Cu nanoparticle/graphene composite at different SOC. (d) Reversible capacities of Mo_6S_8 cathodes with Cu nanoparticle/graphene composite and Si nanoparticle/graphene composite compared to a pristine Mo_6S_8 cathode.

indicating the improvement of the rate capability of the Cu nanoparticle/graphene composite (Figure S8, Supporting Information). This represents another promising feature of Cu nanoparticle/graphene composite, in that the enhanced electrical conductivity provided by the combination of the graphene framework and *in situ* Cu metal coating on the surface of Mo_6S_8 particles leads to better capacity retention even at high current densities over 10 C (1 C = 120 mA/g). It is also interesting that the electrochemical replacement reaction of Cu at 0.75 V vs Mg/Mg^{2+} shows similar polarization to the Mg^{2+} insertion at ca. 1.2 V vs Mg/Mg^{2+} (Figure S8, Supporting Information). The poorer rate performance of the Si nanoparticle/graphene composite electrode was observed at above 3 C rates, and it seems to be attributed to the low electrical conductivity of the Si nanoparticles on the surface of the graphene framework.

To clarify the reaction mechanism of Cu replacement, the structure of Mo_6S_8 was further investigated by various structural analyses at a different state of charge (SOC) during the first cycle: (i) open circuit voltage (OCV) at point A, (ii) after Mg^{2+} insertion at point B, and (iii) after Mg^{2+} extraction at point C, as described in Figure 5a. From the collected *ex situ* XRD pattern of Mo_6S_8 cathode containing Cu nanoparticle/graphene composite at OCV (Figure 5b), we confirmed that the Mo_6S_8 phase and metallic Cu were dominantly observed, together with a trace of $Cu_xMo_6S_8$ phase, which is introduced by the *in situ* intercalation of Cu originated from the Cu nanoparticle/graphene composite.[22] When Mg^{2+} was fully inserted into the Mo_6S_8 structure (point B), the only characteristic peaks of single phase $Mg_2Mo_6S_8$ were observed without any evidence for the $Cu_xMo_6S_8$ phase, indicating that Mg^{2+} insertion induces Cu extraction from $Cu_xMo_6S_8$. On the other hand, it should be noted that the formation of the $CuMo_6S_8$ phase was evident after subsequent Mg^{2+} extraction from the $Mg_2Mo_6S_8$ (point C). This supports that Cu anchored on the surface of graphene can spontaneously participate in electrochemical reactions in the Mo_6S_8 structure (Figure S10, Supporting Information). For further inspection, we also carried out *ex situ* XPS analyses in parallel at different SOC, and the results are provided in Figure 5c. The *ex situ* XPS Cu 2p spectra were carefully fitted with the C 1s spectra at 284.5 eV. The Cu 2p 1/2 signals were clearly observed at 932.4 and 952.3 eV at OCV (point A), which corresponds to monovalent Cu species (Cu^+) because of the *in situ* intercalation of Cu into the Mo_6S_8 structure, which is in well accordance with the XRD result at OCV. Importantly, Mg^{2+} insertion (point B) induces a small shift in the binding energy of Cu 2p components, which are assigned to metallic Cu (Cu^0). The shifted binding energy was reversibly recovered by subsequent Mg^{2+} extraction from the structure. It reveals that Cu has a reversible redox reaction of Cu^0/Cu^+ by electrochemical replacement with Mg^{2+} in the structure. As a result, the reversible capacity of Mo_6S_8 can be increased about 7% by addition of the Cu nanoparticle/graphene composite, as estimated from the galvanostatic charge and discharge profiles (Figure 5d).

Moreover, the change in the microstructure of Mo_6S_8 was examined during Mg^{2+} insertion and extraction. Importantly, we found direct evidence for Cu reduction and deposition on the surface of Mo_6S_8 particles. Figure 6 shows TEM images combined with corresponding FFTs of Mo_6S_8 at different SOC. A typical TEM image of the $Cu_xMo_6S_8$ structure was obtained at OCV in Figure 6a,b. After Mg^{2+} insertion (point B), we found that Cu reduction occurred on the surface of Mo_6S_8 particles by forming Cu crystallites less than 5 nm in size

DOI: 10.1021/am508702j
ACS Appl. Mater. Interfaces 2015, 7, 7016−7024

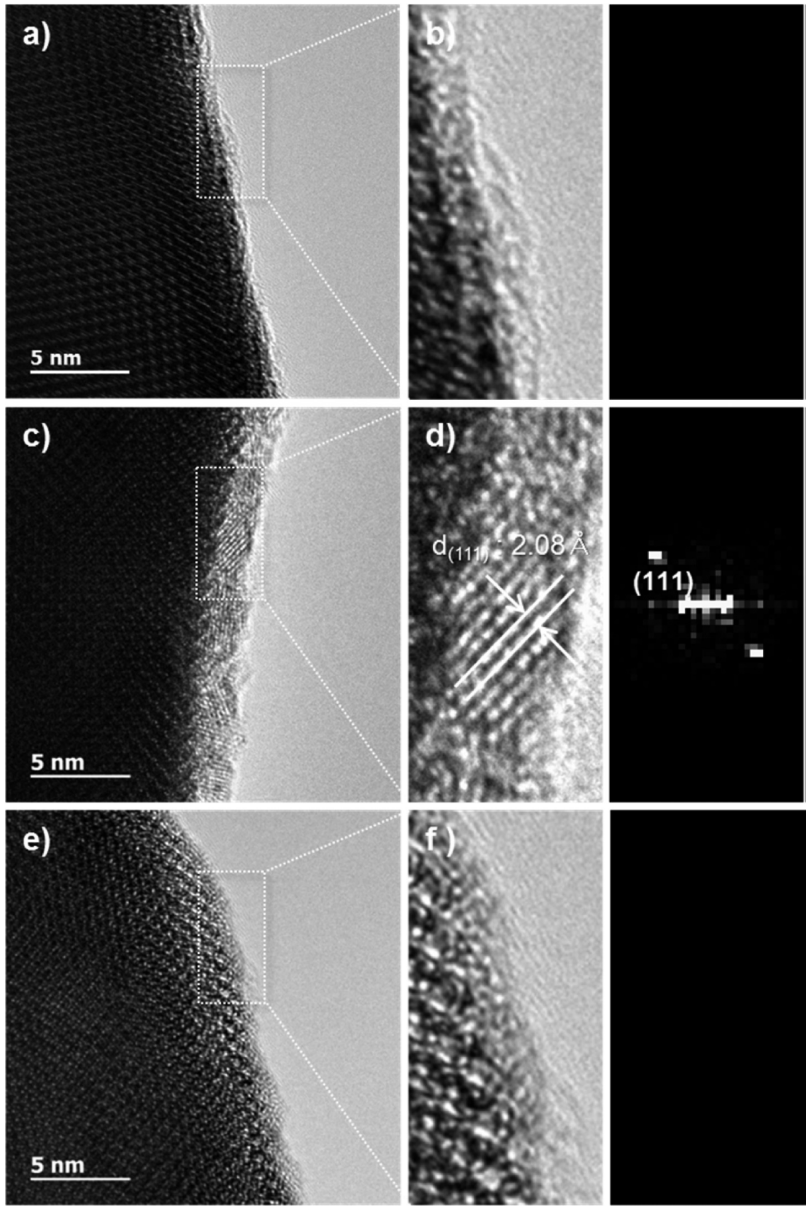

Figure 6. High-resolution TEM images and FFT results of the Mo_6S_8 particle at different SOC; (a, b) OCV (point A), (c, d) after Mg^{2+} insertion (point B), and (e, f) after Mg^{2+} extraction (point C).

(Figure 6c,d). The *d*-spacing was measured to be 2.08 Å, which is well matched with metallic Cu. It reveals that Mg^{2+} insertion extracts Cu^+ from the structure of Mo_6S_8 and extracted Cu^+ is reduced on the surface of Mo_6S_8 particles. After subsequent Mg^{2+} extraction (point C), the Cu crystallite was not detected anymore on the surface of the Mo_6S_8 structure (Figure 6e,f), indicating that Cu is reoxidized and reversibly inserted into the Mo_6S_8 structure along with Mg^{2+} extraction. From those results, we confirm that the reaction of Cu replacement in the Mo_6S_8 structure is allowed by solid state deposition and dissolution of Cu crystallites during cycles, which corresponds to the additional reversible capacity of the Mo_6S_8 cathode at 0.75 V vs Mg/Mg^{2+} during discharge and 1.05 V vs Mg/Mg^{2+} during charge, respectively. Furthermore, we examined whether Cu metal is deposited on the surface of a Mg metal anode after cycling. As evidenced by FESEM and EDS analyses, no Cu species was observed on the Mg metal anode (Figure 7), and this further supports that the additional redox reaction is not attributed to the corrosion of Cu.

CONCLUSIONS

The reversible capacity of Chevrel Mo_6S_8 cathode was increased by the simple addition of Cu nanoparticle/graphene composite. For the Cu metal and Mo_6S_8 mixture electrode, the Cu nanoparticle/graphene composite was obtained by the high temperature plasma synthesis. The electrochemical behaviors of the Mo_6S_8 and Cu mixture cathode were examined with the relevant structural verifications during Mg^{2+} insertion and extraction. The *in situ* formation of $Cu_xMo_6S_8$ was observed, indicating the spontaneous electrochemical insertion of Cu to the Mo_6S_8 structure from the Cu nanoparticle/graphene composite. Moreover, the additional reversible plateau was observed at 0.75 V vs Mg/Mg^{2+} during discharge, which is indicative of a reversible electrochemical replacement reaction of Cu. Further, the reaction mechanism of *in situ* formed

DOI: 10.1021/am508702j
ACS Appl. Mater. Interfaces 2015, 7, 7016−7024

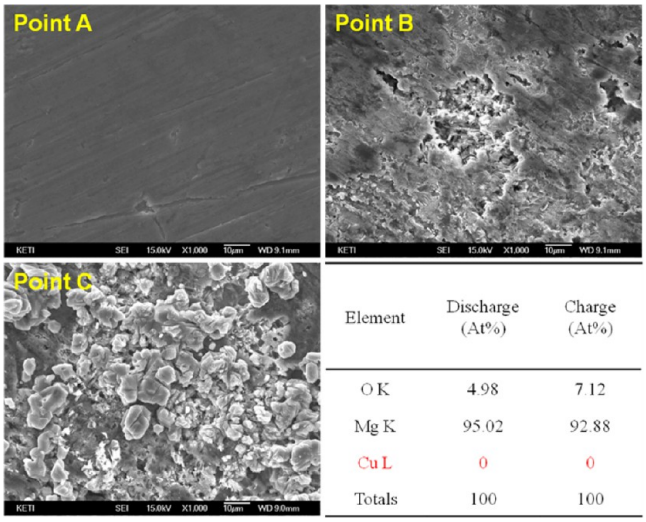

Element	Discharge (At%)	Charge (At%)
O K	4.98	7.12
Mg K	95.02	92.88
Cu L	0	0
Totals	100	100

Figure 7. FESEM images and corresponding EDS results for Mg metal anode at different SOC; (i) OCV (point A), (ii) after Mg^{2+} insertion (point B), and (iii) after Mg^{2+} extraction (point C).

$Cu_xMo_6S_8$ was clarified. During Mg^{2+} insertion, Cu was extracted from the $Cu_xMo_6S_8$ and reduced on the surface of Mo_6S_8 in a form of Cu crystallites in nanoscale. The deposited Cu was reversibly oxidized and reinserted into the Mo_6S_8 structure along with Mg^{2+} extraction during charge. Therefore, the solid state deposition/dissolution of Cu on the surface of Mo_6S_8 is mainly responsible for the additional capacity, and this finding shows great promise for use in practical rechargeable Mg battery applications.

■ ASSOCIATED CONTENT

Supporting Information

Additional FESEM images, schematic diagram, XRD patterns, Raman spectra, XPS, and TEM images. This material is available free of charge via the Internet at http://pubs.acs.org.

■ AUTHOR INFORMATION

Corresponding Authors

*E-mail: parkms@keti.re.kr.
*E-mail: ktlee@snu.ac.kr.

Notes

The authors declare no competing financial interest.

■ ACKNOWLEDGMENTS

This work was supported by the Energy Efficiency & Resources of the Korea Institute of Energy Technology Evaluation and Planning Grant (Project No. 20112010100140) funded by the Korea Government Ministry of Trade, Industry & Energy.

■ REFERENCES

(1) Yang, Z.; Zhang, J.; Kinter-Meyer, M. C. W.; Lu, X.; Choi, D.; Lemmon, J. P.; Liu, J. Electrochemical Energy Storage for Green Grid. *Chem. Rev.* **2011**, *111*, 3577−3613.
(2) Chen, H.; Cong, T. N.; Yang, W.; Tan, C.; Li, Y.; Ding, Y. Progress in Electrical Energy Storage System: A Critical Review. *Prog. Nat. Sci.* **2009**, *19*, 291−312.
(3) Lin, J.; Zhao, L.; Heo, Y. U.; Wang, L.; Bijarbooneh, F. H.; Mozer, A. J.; Nattestad, A.; Yamauchi, Y.; Dou, S. X.; Kim, J. H. Mesoporous Anatase Single Crystals for Efficient $Co^{(2+/3+)}$-Based Dye-Sensitized Solar Cell. *Nano Energy* **2015**, *11*, 557−567.
(4) Pramanik, M.; Tsujimoto, Y.; Malgras, V.; Dou, S. X.; Kim, J. H.; Yamauchi, Y. Mesoporous Iron Phosphonate Electrodes with Crystalline Frameworks for Lithium-Ion Batteries. *Chem. Mater.* **2015**, *27*, 1082−1089.
(5) Tang, J.; Liu, J.; Torad, N. L.; Kimura, T.; Yamauchi, Y. Tailored Design of Functional Nanoporous Carbon Materials toward Fuel Cell Applications. *Nano Today* **2014**, *9*, 305−323.
(6) Goodenough, J. B.; Park, K.-S. The Li-Ion Rechargeable Battery: A Perspective. *J. Am. Chem. Soc.* **2013**, *135*, 1167−1176.
(7) Etacheri, V.; Marom, R.; Elazari, R.; Salitra, G.; Aurbach, D. Challenges in the Development of Advanced Li-Ion Batteries: A Review. *Energy Environ. Sci.* **2011**, *4*, 3243−3262.
(8) Bandhauer, T. M.; Garimella, S.; Fuller, T. F. A Critical Review of Thermal Issues in Lithium-Ion Batteries. *J. Electrochem. Soc.* **2011**, *158*, R1−R25.
(9) Gregory, T. D.; Hoffman, R. J.; Winterton, R. C. Non-Aqueous Electrochemistry of Magnesium. *J. Electrochem. Soc.* **1990**, *137*, 775−780.
(10) Aurbach, D.; Cohen, Y.; Moshkovich, M. The Study of Reversible Magnesium Deposition by *in Situ* Scanning Tunneling Microscopy. *Electrochem. Solid-State Lett.* **2001**, *4*, A113−A116.
(11) Yoo, H. D.; Shterenberg, I.; Gofer, Y.; Gershinsky, G.; Pour, N.; Aurbach, D. Mg Rechargeable Batteries: An On-Going Challenge. *Energy Environ. Sci.* **2013**, *6*, 2265−2279.
(12) Levi, E.; Gofer, Y.; Aurbach, D. On the Way to Rechargeable Mg Batteries: The Challenge of New Cathode Materials. *Chem. Mater.* **2010**, *22*, 860−868.
(13) Mizrahi, O.; Amir, N.; Pollak, E.; Chusid, O.; Marks, V.; Gottlieb, H.; Larush, L.; Zinigrad, E.; Aurbach, D. Electrolyte Solutions with a Wide Electrochemical Window for Rechargeable Magnesium Batteries. *J. Electrochem. Soc.* **2008**, *155*, A103−A109.
(14) Aurbach, D.; Lu, Z.; Schechter, A.; Gofer, Y.; Gizbar, H.; Turgeman, R.; Cohen, Y.; Moshkovich, M.; Levi, E. Prototype Systems for Rechargeable Magnesium Batteries. *Nature* **2000**, *407*, 724−727.
(15) Chusid, O.; Gofer, Y.; Gizbar, H.; Vestfrid, Y.; Levi, E.; Aurbach, D.; Riech, I. Solid-State Rechargeable Magnesium Batteries. *Adv. Mater.* **2003**, *15*, 627−630.
(16) Aurbach, D.; Gofer, Y.; Lu, Z.; Schechter, A.; Chusid, O.; Gizbar, H.; Cohen, Y.; Ashkenazi, V.; Moshkovich, M.; Turgeman, R.; Levi, E. A Short Review on the Comparison between Li Battery Systems and Rechargeable Magnesium Battery Technology. *J. Power Sources* **2001**, *97*, 28−32.
(17) Aurbach, D.; Suresh, G. S.; Levi, E.; Mitelman, A.; Mizrahi, O.; Chusid, O.; Brunelli, M. Progress in Rechargeable Magnesium Battery Technology. *Adv. Mater.* **2007**, *19*, 4260−4267.
(18) Suresh, G. S.; Levi, M. D.; Aurbach, D. Effect of Chalcogen Substitution in Mixed $Mo_6S_{8-n}Se_n$ (n = 0, 1, 2) Chevrel Phases on the Thermodynamics and Kinetics of Reversible Mg Ions Insertion. *Electrochim. Acta* **2008**, *53*, 3889−3896.
(19) Woan, K.; Scheffler, R.; Bell, N.; Sigmund, W. Electrospinning of Nanofiber Chevrel Phase Materials. *J. Mater. Chem.* **2011**, *21*, 8537−8539.
(20) Levi, E.; Gofer, Y.; Vestfreed, Y.; Lancry, E.; Aurbach, D. $Cu_2Mo_6S_8$ Chevrel Phase, A Promising Cathode Material for New Rechargeable Mg Batteries: A Mechanically Induced Chemical Reaction. *Chem. Mater.* **2002**, *14*, 2767−2773.
(21) Mitelman, A.; Levi, M. D.; Lancry, E.; Levi, E.; Aurbach, D. New Cathode Materials for Rechargeable Mg Batteries: Fast Mg Ion Transport and Reversible Copper Extrusion in $Cu_yMo_6S_8$ Compounds. *Chem. Commun.* **2007**, 4212−4214.
(22) Woo, S. G.; Yoo, J. Y.; Cho, W.; Park, M.-S.; Kim, K. J.; Kim, J.-H.; Kim, J.-S.; Kim, Y.-J. Copper Incorporated $Cu_xMo_6S_8$ ($x \geq 1$) Chevrel Phase Cathode Materials Synthesized by Chemical Intercalation Process for Rechargeable Magnesium Batteries. *RSC Adv.* **2014**, *4*, 59048−59055.
(23) Chevrel, R.; Sergent, M.; Prigent, J. Un Nouveau Sulfure De Molybdene: Mo_3S_4 Preparation, Proprietes Et Structure Cristalline. *Mater. Res. Bull.* **1974**, *9*, 1487−1498.

DOI: 10.1021/am508702j
ACS Appl. Mater. Interfaces 2015, 7, 7016−7024

(24) Levi, E.; Gershinsky, G.; Aurbach, D.; Isnard, O.; Ceder, G. New Insight on the Unusually High Ionic Mobility in Chevrel Phases. *Chem. Mater.* **2009**, *21*, 1390−1399.
(25) Lancry, E.; Levi, E.; Gofer, Y.; Levi, M.; Salitra, G.; Aurbach, D. Leaching Chemistry and the Performance of the Mo_6S_8 Cathodes in Rechargeable Mg Batteries. *Chem. Mater.* **2004**, *16*, 2832−2838.
(26) Jinschek, J. Advances in the Environmental Transmission Electron Microscope (ETEM) for Nanoscale *in Situ* Studies of Gas−Solid Interactions. *Chem. Commun.* **2014**, *50*, 2696−2706.
(27) Salavati-Niasari, M.; Davar, F. Synthesis of Copper and Copper (I) Oxide Nanoparticles by Thermal Decomposition of a New Precursor. *Mater. Lett.* **2009**, *63*, 441−443.
(28) Zhao, W.; Fang, M.; Wu, F.; Wu, H.; Wang, L.; Chen, G. Preparation of Graphene by Exfoliation of Graphite Using Wet Ball Milling. *J. Mater. Chem.* **2010**, *20*, 5817−5819.
(29) Ci, L.; Zhu, H.; Wei, B.; Xu, C.; Wu, D. Annealing Amorphous Carbon Nanotubes for Their Application in Hydrogen Storage. *Appl. Surf. Sci.* **2003**, *205*, 39−43.
(30) Chusuei, C. C.; Broolshier, M. A.; Goodman, D. W. Correlation of Relative X-ray Photoelectron Spectroscopy Shake-up Intensity with CuO Particle Size. *Langmuir* **1999**, *15*, 2806−2808.

DOI: 10.1021/am508702j
ACS Appl. Mater. Interfaces 2015, 7, 7016−7024